Electronic Supplementary Material (ESI) for Dalton Transactions.

Supplementary Material

Luminescence thermometry in a Dy_4 single molecule magnet

Julio Corredoira-Vázquez,[a,b] Cristina González-Barreira,[a] Matilde Fondo,[a,*] Ana M. García Deibe,[a] Jesús Sanmartín Matalobos,[a,c] Miguel A. Hernández-Rodríguez,[b] Luís D. Carlos[b,*]

[a] *Departamento de Química Inorgánica, Facultade de Química, Universidade de Santiago de Compostela, Campus Vida, 15782 Santiago de Compostela, Spain.*

[b] *Phantom-g, CICECO – Aveiro Institute of Materials, Department of Physics, University of Aveiro, 3810-193 – Aveiro, Portugal.*

[c] *Institute of Materials (iMATUS), Universidade de Santiago de Compostela, 15782 Santiago de Compostela, Spain*

Table S1. Crystal data and structure refinement for **1**·CH_3OH.

Empirical formula	$C_{67}H_{88}Dy_4N_8O_{19}$
Molecular weight	1959.45
Crystal system	Monoclinic
Space group	$P2_1/c$
Wavelength (Å)	0.71073
Crystal size (mm^3)	0.090 x 0.070 x 0.050
Colour, shape	Colourless, prism
T (K)	100(2)
a (Å)	16.2186(15)
b (Å)	13.5792(10)
c (Å)	17.0915(15)
α (º)	90
β (º)	105.691(3)
γ (º)	90
Volume (Å^3)	3623.9(5)
Z	2
Absorpt. coef. (mm^{-1})	4.150
Reflections collected	74882
Independent reflections	7400 [R_{int} = 0.1037]
Data / restraints / param.	7400 / 0 / 445
Final R indices [$I>2\sigma(I)$]	R_1 = 0.0410; wR_2 = 0.0729
R indices (all data)	R_1= 0.0646; wR_2 = 0.0823

Table S2. Main bond distances (Å) and angles (º) for **1**·CH_3OH.

Dy1-O11	2.333(4)	Dy2-O11	2.347(4)
Dy1-O13	2.290(4)	Dy2-O13	2.346(4)
Dy1-O12	2.215(4)	Dy2-O2	2.317(5)
Dy1-O1	2.356(4)	Dy2-O3	2.307(4)
Dy1-N13	2.571(5)	Dy2-O4$^{\#1}$	2.332(4)
Dy1-N12	2.574(5)	Dy2-O5	2.363(4)
Dy1-N14	2.581(5)	Dy2-O6$^{\#1}$	2.468(5)
Dy1-N11	2.676(5)	Dy2-O5$^{\#1}$	2.481(4)
Dy1···Dy2	3.7561(5)	Dy2···Dy2$^{\#1}$	3.8274(6)
O13-Dy1-N12	153.90(16)	O2-Dy2-O6$^{\#1}$	157.59(16)
N13-Dy1-N12	66.58(17)	O6$^{\#1}$-Dy2-O5$^{\#1}$	52.26(14)
Dy1-O11-Dy2	106.77(16)	Dy2-O5-Dy2$^{\#1}$	104.38(16)
Dy1-O13-Dy2	108.23(16)		

Table S3. SHAPE v2.1. Continuous shape measures calculation (c) 2013 Electronic Structure Group, Universitat de Barcelona.

Geometries Coordination number 8

ETBPY-8	13 D3h	Elongated trigonal bipyramid
TT-8	12 Td	Triakis tetrahedron
JSD-8	11 D2d	Snub diphenoid J84
BTPR-8	10 C2v	Biaugmented trigonal prism
JBTPR-8	9 C2v	Biaugmented trigonal prism J50
JETBPY-8	8 D3h	Johnson elongated triangular bipyramid J14
JGBF-8	7 D2d	Johnson gyrobifastigium J26
TDD-8	6 D2d	Triangular dodecahedron
SAPR-8	5 D4d	Square antiprism
CU-8	4 Oh	Cube
HBPY-8	3 D6h	Hexagonal bipyramid
HPY-8	2 C7v	Heptagonal pyramid
OP-8	1 D8h	Octagon

Dy1

Structure [ML8]	ETBPY-8	TT-8	**JSD-8**	BTPR-8	JBTPR-8	JETBPY-8	JGBF-8
	21.354,	12.504,	**2.910**,	3.635,	3.346,	26.824,	8.949,

TDD-8	SAPR-8	CU-8	HBPY-8	HPY-8	OP-8
1.802,	4.433,	12.272,	14.405,	22.175,	30.011

Dy2

Structure [ML8]	ETBPY-8	TT-8	JSD-8	BTPR-8	JBTPR-8	JETBPY-8	JGBF-8
	22.859,	10.419,	4.944,	2.545,	2.936,	27.699,	15.018,

TDD-8	**SAPR-8**	CU-8	HBPY-8	HPY-8	OP-8
2.045,	**1.479**,	9.712,	15.000,	21.727,	30.185

Table S4. Temperature (*T*), maximum intensities (I_i, *i=1.2*), readout fluctuation of the baseline (δI), relative uncertainty in intensities ($\delta I/I_i$, *i=1.2*), relative uncertainty in Δ ($\delta\Delta/\Delta$), relative thermal sensitivity (S_r) and temperature uncertainty (δT).

T	I_1	I_2	δI	$\delta I/I_1$	$\delta I/I_2$	$\delta\Delta/\Delta$	S_r	δT
K	10^6 arb. units		10^6				$\%.K^{-1}$	*K*
11	2.88	1.24	0.0066	0.0023	0.0053	0.0058	0.1	16.6
50	2.42	1.06	0.0072	0.0030	0.0068	0.0075	0.2	8.9
100	2.17	0.91	0.0089	0.0041	0.0097	0.0105	0.4	4.3
150	1.95	0.85	0.0089	0.0046	0.0105	0.0114	0.7	2.4
200	2.01	0.86	0.0097	0.0048	0.0113	0.0123	1.1	1.6
250	2.02	0.76	0.0110	0.0054	0.0144	0.0154	1.4	1.2
295	2.11	0.82	0.0132	0.0063	0.0162	0.0174[a]	1.6	1.1

[a]Maximum value considered for the estimation of δT.

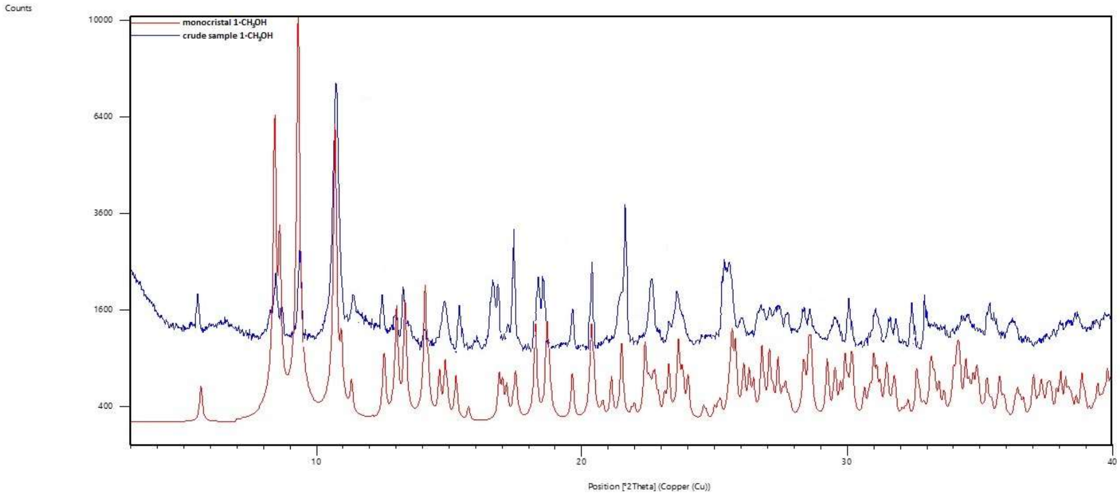

Fig. S1. Comparison of X-powder diffractogram for the crystalline sample of **1**·CH_3OH with the simulated one from single X-ray data.

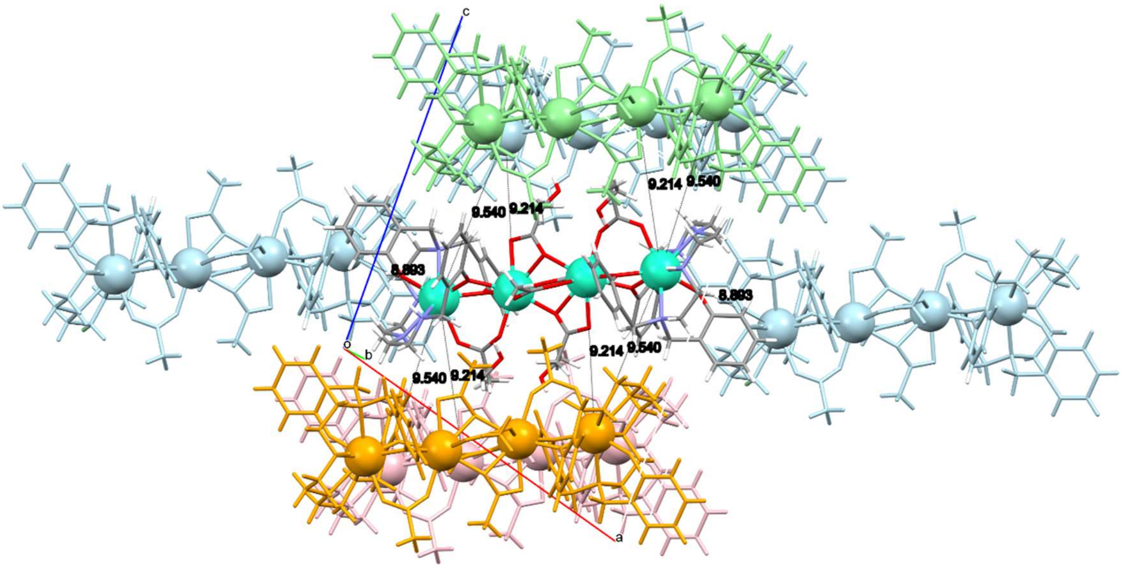

Fig. S2. Crystal packing for **1**·CH_3OH, showing the shortest Dy···Dy intermolecular distances.

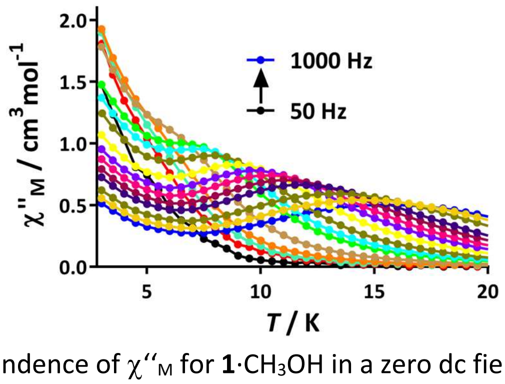

Fig. S3. Temperature dependence of χ''_M for **1**·CH_3OH in a zero dc field at different frequencies.

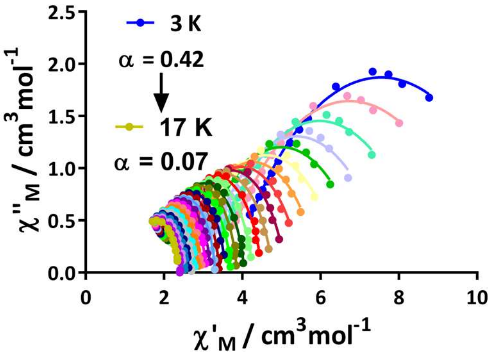

Fig. S4. Cole-Cole plot for **1**·CH_3OH in H_{dc} = 0.

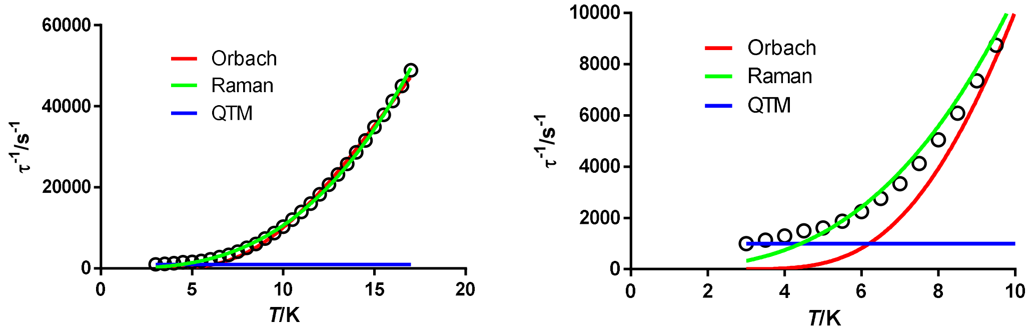

Fig. S5. τ^{-1} versus *T* plot for **1**·CH_3OH in a zero dc field showing the Orbach, Raman, and QTM contribution tos the fit: left) in the temperature range 3-17 K; right) in the temperature range 3-10 K.

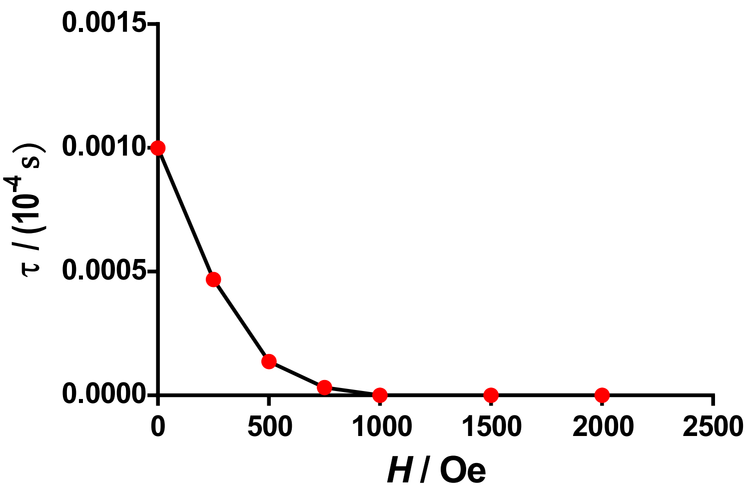

Fig. S6. Dependence of the relaxation time with the field for **1**·CH_3OH at 3 K.

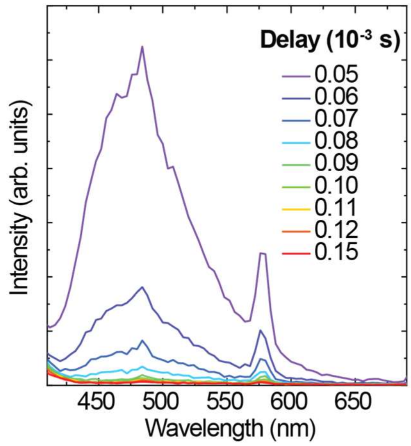

Fig. S7. Temperature dependence of the **1**·CH_3OH sample time resolved emission recorded at 11 K for different starting delays.

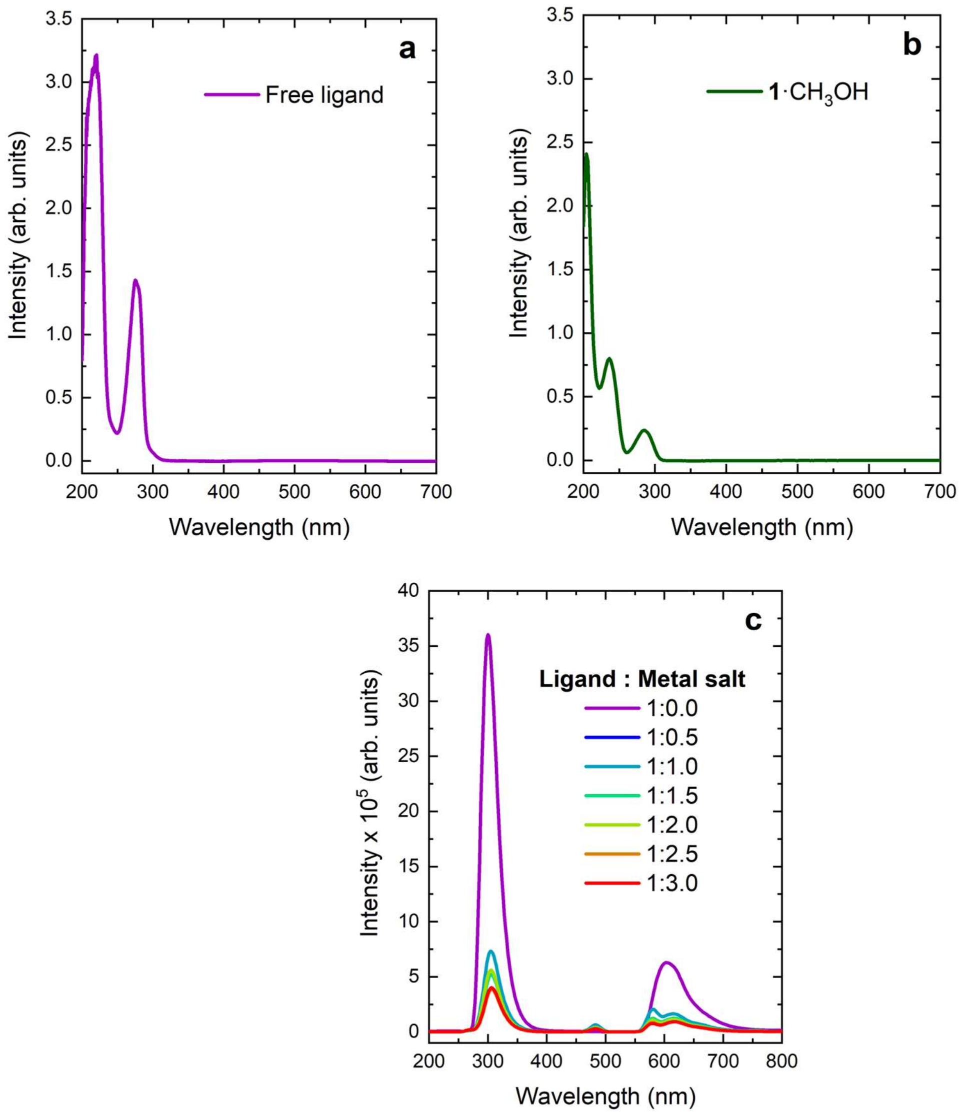

Fig. S8. (a) Absorption spectrum of the free ligand **(a)** and of 1·CH_3OH **(b)** in a methanolic solution. **(c)** Emission spectra of $H_6L_c^r$-Dy salt mixtures in methanolic solutions for different ligand to metal salt ratios upon 274 nm excitation recorded at room temperature.

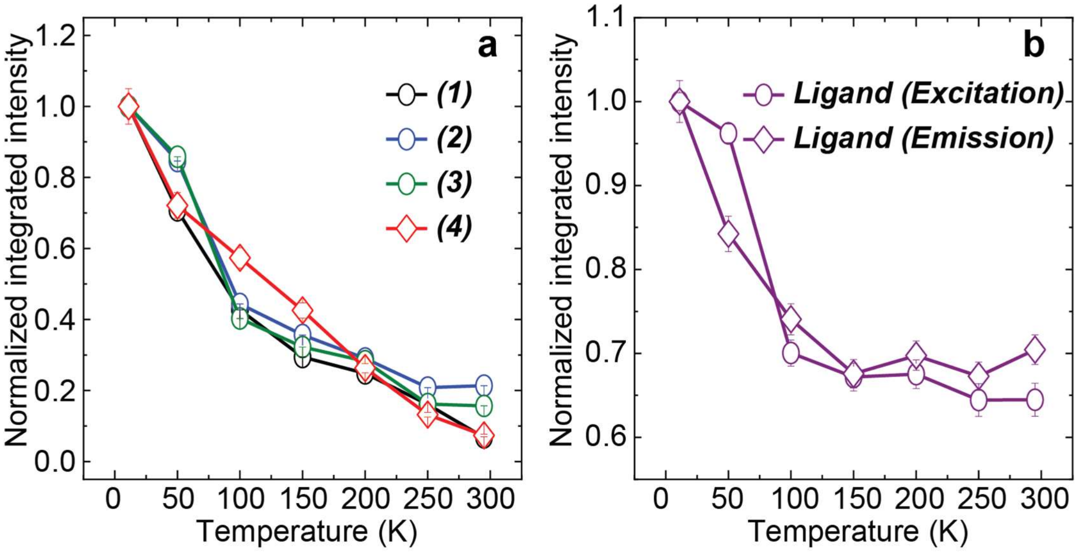

Fig. S9. (a) Temperature dependence of the normalized integrated intensities of the Dy emission (diamond red symbols) and excitation (circular symbols) related bands. *(1)*, *(2)* and *(3)* represent the normalized integrated excitation intensity of the $^6H_{15/2} \rightarrow {}^4K_{15/2}$; $^6H_{15/2} \rightarrow {}^4M_{15/2}, {}^6P_{7/2}$ and $^6H_{15/2} \rightarrow {}^4I_{15/2}$ transitions respectively, whereas *(4)* normalized integrated emission intensity ascribed to the $^4F_{9/2} \rightarrow {}^6H_{13/2}$ transition. **(b)** Temperature dependence of the normalized integrated intensities of the ligand emission (diamond purple symbols) and excitation (circular purple symbols) related bands.